Magnetic symmetries in neutron and resonant x-ray Bragg diffraction patterns of four iridium oxides

2012 J. Phys.: Condens. Matter 24 496003

(http://iopscience.iop.org/0953-8984/24/49/496003)

J. Phys.: Condens. Matter **24** (2012) 496003 (10pp) doi:10.1088/0953-8984/24/49/496003

Magnetic symmetries in neutron and resonant x-ray Bragg diffraction patterns of four iridium oxides

S W Lovesey[1,2], D D Khalyavin[1], P Manuel[1], L C Chapon[3], G Cao[4] and T F Qi[4]

[1] ISIS Facility, STFC, Didcot, Oxfordshire OX11 0QX, UK
[2] Diamond Light Source Ltd, Harwell Science and Innovation Campus, Oxfordshire OX11 0DE, UK
[3] Institute Laue-Langevin, BP 156, F-38042 Grenoble Cedex 9, France
[4] Department of Physics and Astronomy, University of Kentucky, Lexington, Kentucky 40506, USA

Received 2 October 2012, in final form 29 October 2012
Published 16 November 2012
Online at stacks.iop.org/JPhysCM/24/496003

Abstract
The magnetic properties of Sr_2IrO_4, Na_2IrO_3, $Sr_3Ir_2O_7$ and $CaIrO_3$ are discussed, principally in the light of experimental data in recent literature for Bragg intensities measured in x-ray diffraction with enhancement at iridium L-absorption edges. The electronic structure factors we report, which incorporate parity-even and acentric entities, serve the immediate purpose of making full use of crystal and magnetic symmetry to refine our knowledge of the magnetic properties of the four iridates from resonant x-ray diffraction data. They also offer a platform on which to interpret future investigations, using dichroic signals, resonant x-ray diffraction and neutron diffraction, for example, as well as *ab initio* calculations of electronic structure. Unit-cell structure factors, suitable for x-ray Bragg diffraction enhanced by an electric dipole–electric dipole (E1–E1) event, reveal exactly which iridium multipoles are visible, e.g., a magnetic dipole parallel to the crystal *c*-axis (*z*-axis) and an electric quadrupole with *yz*-like symmetry in the specific case of $CaIrO_3$. Magnetic space-groups are assigned to Sr_2IrO_4, $Sr_3Ir_2O_7$ and $CaIrO_3$, namely, P_Icca, P_Aban and $Cm'cm'$, respectively, in the Belov–Neronova–Smirnova notation. The assignment for Sr_2IrO_4 is possible because of our new high-resolution neutron diffraction data, gathered on a powder sample. In addition, the new data are used to show that the ordered magnetic moment of an Ir^{4+} ion in Sr_2IrO_4 does not exceed 0.29(4) μ_B. Na_2IrO_3 has two candidate magnetic space-groups that are not resolved with currently available resonant x-ray data.

(Some figures may appear in colour only in the online journal)

1. Introduction

It is fashionable to study magnetic properties of platinum (5d) transition-metal oxides that contain iridium (Ir^{4+}, $5d^5$) using experimental and theoretical techniques [1–15]. Novelty and a real possibility that knowledge gained from the studies will find application in devices and quantum computation drives the current scientific quest. Materials of interest are insulating, not withstanding of largely extended 5d-orbitals that favour a metallic phase (their counterparts in the ruthenates are metallic or even superconducting), and the paramagnetic susceptibility either does not follow a Curie–Weiss law or fitting to such a law gives an unexpected Weiss constant and effective moment, although this particular puzzle for Na_2IrO_3 has an answer [15]. A partially occupied orbital in the low-spin t^5 configuration is a one-electron state, a situation which accentuates quantum effects that are non-commonsensical. Total angular momentum is a good quantum number—the strength of the spin–orbit coupling increases with atomic number Z for d electrons of a given column of the Periodic table—meaning that cation spin and orbital degrees of freedom are inseparables in platinum compounds. In contrast, orbital degeneracy does not usually survive in 3d oxides, where eigen-states of the crystal-field

potential are purely real and orbital angular momentum is quenched or much reduced making typically no more than a 10% contribution to the magnetic moment.

The experimental technique of x-ray Bragg diffraction enhanced by an atomic resonance has been used to great effect in recent studies of magnetic properties of iridates [4, 6, 7, 11, 13]. (The efficacy of neutron diffraction is diminished by strong Ir absorption.) Tuning the primary x-ray energy to iridium L-edges ($L_2 \approx 12.82$ keV and $L_3 \approx 11.21$ keV) yields direct information from Bragg intensities on charge, spin and orbital degrees of freedom in 5d-orbitals, when absorption proceeds via an electric-dipole transition (E1). A feature of particular relevance is that, orbital angular momentum is observed when intensity at one absorption edge is zero, as is often found to be the case. Stringent conditions on the magnetic space-group can be derived from published diffraction data taken together with bulk properties, as we shall demonstrate with four iridates in this communication.

To interpret published data, we exploit an atomic model of resonant x-ray scattering that is convenient to make best use of symmetry, symmetry within the scattering process and symmetry imposed by physical properties of the crystal (Neumann's principle) [16–19]. Two of the four iridates, Sr_2IrO_4 [4] and Na_2IrO_3 [6], are the subjects of previous successful investigations [14, 15]. Here, we add additional information, particularly about Sr_2IrO_4 with magnetic propagation vector (1, 1, 1). Using new data gathered on a powder sample of Sr_2IrO_4 by neutron diffraction, in conjunction with published x-ray data [4], we can assign a bi-dimensional irreducible representation M_4 and a magnetic space-group P_Icca ($I_pb'ca$), specified in terms of the Miller and Love notation and Belov–Neronova–Smirnova and Opechowski–Guccione (in brackets) notations. X-ray diffraction data for the two remaining iridates in this communication, $Sr_3Ir_2O_7$ [11] and $CaIrO_3$ [13], have not previously been interpreted by us. We show that extensive published data [11] gathered on magnetically ordered $Sr_3Ir_2O_7$ are entirely consistent with one of two candidate magnetic space-groups, namely, P_Aban (C_pcca) with magnetic propagation vector at Y-point of symmetry (1, 0, 0). In addition to this, we demonstrate conditions on the iridium wavefunction necessary to match observed intensities. While for $CaIrO_3$ [13] we establish a magnetic propagation vector $= 0$ at the Γ–point of symmetry (in this case, the two notations, Belov–Neronova–Smirnova and Opechowski–Guccione, coincide). Published observations of x-ray Bragg diffraction permit us to make an unambiguous assignment of the magnetic space-group, $Cm'cm'$ with a ferromagnetic component parallel to the b-axis and an antiferromagnetic motif of magnetic dipoles aligned along the c-axis. For all four materials we construct electronic structure factors in terms of atomic multipoles that describe parity-even and, when allowed by an absence of symmetry, acentric magnetic properties.

Section 2 is a précis of the case for and properties of atomic multipoles in the interpretation of resonant x-ray diffraction and absorption (dichroic signals). Thereafter, we work through magnetic properties of the four mentioned iridates. Findings are gathered and discussed in section 7.

2. Multipoles

An atomic multipole is a property of the ground-state of a material, and it encapsulates electron charge, spin and orbital degrees of freedom [16–19]. Using angular brackets $\langle\cdots\rangle$ to denote the expectation value of the enclosed operator, $\langle O^K_Q\rangle = \langle O^K_Q\rangle' + \mathrm{i}\langle O^K_Q\rangle''$ is a spherical, atomic multipole of integer rank K and projection Q ($-K \le Q \le K$) with parity signature $\sigma_\pi = \pm 1$. The complex conjugate obeys $\langle O^K_Q\rangle^* = (-1)^Q\langle O^K_{-Q}\rangle$ with $\langle O^K_0\rangle$ purely real. Rotations around orthogonal axes by 180° yield $C_{2x}\langle O^K_Q\rangle = (-1)^K\langle O^K_{-Q}\rangle$, $C_{2y}\langle O^K_Q\rangle = (-1)^{K+Q}\langle O^K_{-Q}\rangle$, and $C_{2z}\langle O^K_Q\rangle = \exp(\mathrm{i}\pi Q)\langle O^K_Q\rangle = (-1)^Q\langle O^K_Q\rangle$.

Parity-even resonant events, such as dipole–dipole (E1–E1) and quadrupole–quadrupole (E2–E2), are described with multipoles $\langle T^K_Q\rangle$ that have $\sigma_\pi = +1$ and a time signature $\sigma_\theta = (-1)^K$. Two types of multipole are used for parity-odd resonant events, including electric dipole–magnetic dipole (E1–M1) and dipole–quadrupole (E1–E2). Both multipoles have $\sigma_\pi = -1$, of course, with $\langle G^K_Q\rangle$ time-odd ($\sigma_\theta = -1$) and $\langle U^K_Q\rangle$ time-even ($\sigma_\theta = +1$) [16–19].

Physical properties of $\langle T^K_Q\rangle$ are discussed by Carra *et al* [20] and Lovesey and Balcar [21]. For the moment, it is enough to quote sum-rules for integrated intensities at L_2 and L_3 absorption edges. For magnetic dipole moments ($K = 1$),

$$\langle \mathbf{T}^1\rangle_{L2} + \langle \mathbf{T}^1\rangle_{L3} = -\langle \mathbf{L}\rangle_{\mathrm{d}}/(10\sqrt{2}), \tag{2.1}$$

where $\langle \mathbf{L}\rangle_{\mathrm{d}}$ is orbital angular momentum in the nd-valence state. Note that Cartesian components and spherical components of a dipole $\mathbf{R}$ are related by $R_x = (R_{-1} - R_{+1})/\sqrt{2}$, $R_y = \mathrm{i}(R_{-1} + R_{+1})/\sqrt{2}$, and $R_z = R_0$. The corresponding quadrupole ($K = 2$) sum-rule is,

$$\langle \mathbf{T}^2\rangle_{L2} + \langle \mathbf{T}^2\rangle_{L3} = \langle\{\mathbf{L}\otimes\mathbf{L}\}^2\rangle_{\mathrm{d}}/60, \tag{2.2}$$

where the tensor product $\{\mathbf{L}\otimes\mathbf{L}\}^2$ has for its diagonal component ($Q = 0$) a value $\{\mathbf{L}\otimes\mathbf{L}\}^2_0 = [3L_z^2 - L(L+1)]/\sqrt{6}$, which demonstrates affinity to a standard, parity-even quadrupole operator.

Turning to magneto-electric multipoles, $\langle G^K_Q\rangle$, we cite the sum-rule for anapoles ($K = 1$) [24]. This involves the expectation value of the electric-dipole, $\mathbf{R}$, in a vector product with the magnetic moment, $\mu = (\mathbf{L} + 2\mathbf{S})$, namely,

$$\langle \mathbf{G}^1\rangle_{L2} + \langle \mathbf{G}^1\rangle_{L3} = -\langle(\mathbf{R}\times\mu)\rangle_{\mathrm{d}}/(2\sqrt{2}). \tag{2.3}$$

Magnetic charge, $\langle G^0_0\rangle$, can contribute to an E1–M1 event for which $K = 0$–2.

Figure 1 illustrates the geometry of an x-ray Bragg diffraction experiment. In the Bragg setting, primary and secondary wavevectors satisfy $\mathbf{q} - \mathbf{q}' = (h, k, l)$ where h, k, l are Miller indices, and θ is the Bragg angle. In line with current practice, σ labels primary polarization normal to the plane of scattering and π' labels secondary polarization parallel to the plane.

A unit-cell structure factor, F, suitable for the interpretation of Bragg diffraction patterns created with x-rays or

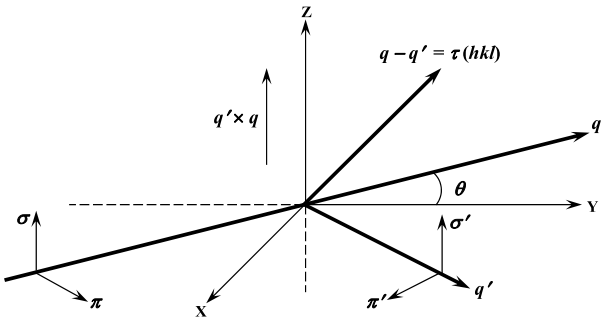

Figure 1. The diagram illustrates the Cartesian coordinate system (x, y, z) adopted for Bragg diffraction and the relation to states of polarization, σ and π, in the primary (unprimed) and secondary (primed) beams of x-rays. The beam is deflected through and angle 2θ, and $\mathbf{q}$ and $\mathbf{q}'$ are primary and secondary wavevectors.

neutrons is constructed from [16],

$$\Psi^K_Q = \sum_{\mathbf{d}} \exp(\mathrm{i}\mathbf{d}\cdot\mathbf{k})\langle O^K_Q\rangle_{\mathbf{d}}, \tag{2.4}$$

where the sum is over all (resonant) ions at position $\mathbf{d}$ in the unit cell, and the scattering wavevector $\mathbf{k} = (h, k, l)$. Magnetization, dichroic signals and other bulk properties allowed by the crystal-class are described by Ψ^K_Q evaluated with $\mathbf{k} = 0$. On the other hand, elements of the full magnetic space-group appear in Bragg diffraction, which consequently provides more information on a crystal than a bulk property.

Universal expressions for F, in all four polarization channels of resonant x-ray diffraction $(\sigma'\sigma, \sigma'\pi, \pi'\sigma, \pi'\pi)$, are presented neatly in terms of quantities A^K_Q and B^K_Q that are even and odd functions of Q, namely, $A^K_Q = (\Psi^K_Q + \Psi^K_{-Q})/2$ and $B^K_Q = (\Psi^K_Q - \Psi^K_{-Q})/2$, with Ψ^K_Q evaluated in the setting depicted in figure 1 (possibly chosen as the origin of an azimuthal-angle scan). All unit-cell structure factors for E1–E1, E1–E2 and E2–E2 events are catalogued by Scagnoli and Lovesey [17] and corresponding results for E1–M1 by Lovesey and Scagnoli [18].

3. Sr_2IrO_4

Space-group $I4_1/acd$ (#142), tetragonal, centrosymmetric crystal-class D_{4h} $(4/mmm)$, with origin choice 2, and body-centring $(\frac{1}{2}, \frac{1}{2}, \frac{1}{2})$. Ir ions occupy sites 8(a) $\frac{1}{2}, \frac{1}{4}, \frac{1}{8}$; $0, \frac{3}{4}, \frac{1}{8}$; $\frac{1}{2}, \frac{3}{4}, \frac{3}{8}$; $0, \frac{1}{4}, \frac{3}{8}$ that are not centres of inversion symmetry, and the point group is $IC_{4c}(\bar{4})$.

A magnetic dipole is an axial quantity and unchanged by inversion, I. Thus $IC_{4c}\langle T^1_Q\rangle = C_{4c}\langle T^1_Q\rangle = \exp(\mathrm{i}\pi Q/2)\langle T^1_Q\rangle = \langle T^1_Q\rangle$ is satisfied by $Q = 0$ and the dipole is parallel to the c-axis. This finding disagrees with experimental data, which are consistent with magnetic dipoles normal to the c-axis. The appropriate point group is $C'_{2c}\langle T^K_Q\rangle = \theta C_{2c}\langle T^K_Q\rangle = (-1)^{K+Q}\langle T^K_Q\rangle = \langle T^K_Q\rangle$, where θ denotes the operation of reversing the direction of time. On the other hand, $C'_{2c}\langle G^K_Q\rangle = -(-1)^Q\langle G^K_Q\rangle = \langle G^K_Q\rangle$, since $\sigma_\theta\ (= \sigma_\pi) = -1$. Given Q odd for all K the anapole (toroidal dipole) with $Q = \pm 1$ is likewise normal to the c-axis, while magnetic charge, $\langle G^0_0\rangle$, is a forbidden acentric magnetic multipole.

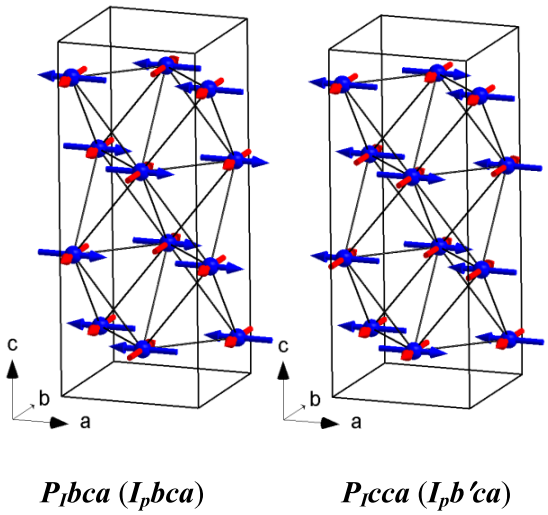

Figure 2. Sr_2IrO_4; magnetic dipole components in the a–b plane associated with M_3 (left) and M_4 (right) irreps.

3.1. Resonant x-ray Bragg diffraction

Resonant x-ray Bragg diffraction data for the K_2NiF_4-type single-layer perovskite at space-group forbidden reflections are reported by Kim *et al* [4]. In the absence of an applied magnetic field, intensity is observed at (h, k, l) with integer Miller indices, $h + k + l$ odd and space-group forbidden; specifically, $(0, 1, 4n+2)$, $(1, 0, 4n)$ and $(0, 0, 2n+1)$. (Direct resonant inelastic x-ray scattering with full momentum dependence is the subject of [22, 23].)

A body-centring anti-translation $\theta(\frac{1}{2}, \frac{1}{2}, \frac{1}{2})$ is necessary with magnetic propagation vector (1, 1, 1) [14]. Using group-theoretical methods implemented into ISOTROPY [30] and ISODISTORT [31] software, different magnetic dipole configurations transforming as basis functions of irreducible representations (irreps) associated with this propagation vector have been systematically studied. Two bi-dimensional irreps M_3 and M_4 with equal components of the corresponding order parameters resulting in the P_Ibca (I_pbca) and P_Icca $(I_pb'ca)$ magnetic space-groups are consistent with the observed reflection conditions and they are not distinguished in resonant Bragg diffraction. The allowed magnetic dipole components in the a–b plane for these two cases are shown in figure 2. In consequence, motifs of magnetic dipoles in this plane are $+, +, -, -$ (a-component) and $+, -, +, -$ (b-component) for M_3, and $+, -, +, -$ (a-component) and $+, +, -, -$ (b-component) for M_4.

Using $\sigma_\pi = +1$, corresponding electronic structure factors are,

$$\begin{aligned} M_3;\ \Psi^K_Q &= 2(-1)^h \exp(\mathrm{i}\pi k/2) \\ &\times [\exp(\mathrm{i}\varphi) + (-1)^Q(-1)^{h+l}\exp(-\mathrm{i}\varphi)] \\ &\times [\langle T^K_Q\rangle + (-1)^K(-1)^{h+k}\langle T^K_{-Q}\rangle], \end{aligned} \tag{3.1}$$

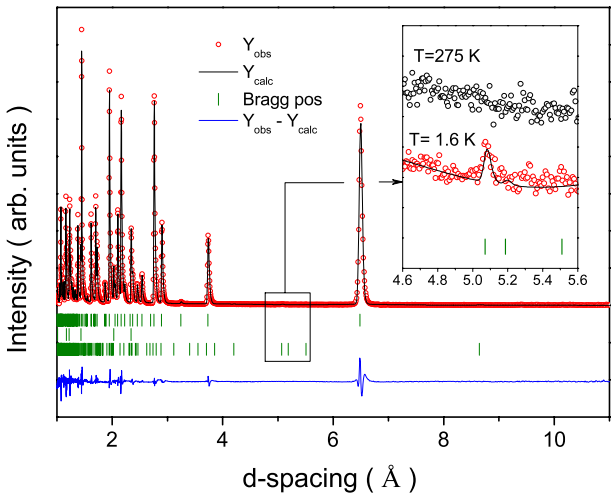

Figure 3. Sr_2IrO_4; Rietveld refinement of the neutron diffraction data measured at 1.6 K. Inset shows two patterns collected at different temperatures near the position where the strongest (1, 0, 2) magnetic reflection is observed.

and,

$$M_4;\ \Psi^K_Q = 2(-1)^h \exp(\mathrm{i}\pi k/2) \times [\exp(\mathrm{i}\varphi) + (-1)^Q(-1)^{h+l}\exp(-\mathrm{i}\varphi)] \times [\langle T^K_Q\rangle + (-1)^{K+Q}(-1)^{h+k}\langle T^K_{-Q}\rangle], \quad (3.2)$$

where $\varphi = \pi l/4$. There are two cases: (a) charge reflections with $h+k+l$ even and multipoles $\langle \mathbf{T}^K\rangle$ with K even unchanged by IC_{4c}, and (b) magnetic reflections with $h + k + l$ odd and multipoles $\langle \mathbf{T}^K\rangle$ with K odd unchanged by C'_{2c}, which requires Q odd. The latter condition on Q tells us that M_3 and M_4 represent diffraction from orthogonal components of $\langle \mathbf{T}^1\rangle$. For (3.1) and (3.2) differ in a factor $(-1)^Q$ between $\langle T^K_Q\rangle$ and $\langle T^K_{-Q}\rangle$, and nothing more, and $\langle T^1_1\rangle + \langle T^1_{-1}\rangle = -\mathrm{i}\sqrt{2}\langle T^1_b\rangle$ while $\langle T^1_1\rangle - \langle T^1_{-1}\rangle = -\sqrt{2}\langle T^1_a\rangle$. In the absence of prior knowledge about $\langle T^1_a\rangle$ and $\langle T^1_b\rangle$ resonant x-ray diffraction does not distinguish M_3 from M_4.

Unit-cell structure factors for diffraction enhanced by an E1–E1 event found in Chapon and Lovesey [14] are derived from (3.2). Structure factors for M_3 are obtained by an exchange $\langle T^1_a\rangle \Leftrightarrow \langle T^1_b\rangle$ in the reported M_4 structure factors.

3.2. Neutron powder diffraction

Since our analysis of resonant x-ray diffraction data in combination with symmetry arguments did not resolve the two magnetic motifs shown in figure 2, we performed a suitable neutron diffraction experiment. The measurements were done on 1 g powder sample using a time-of-flight diffractometer, WISH, located at the ISIS facility, Rutherford Appleton Laboratory (UK). In spite of the large absorption cross section of Ir, our data in figure 3 are of high quality with very low background, achieved by appropriate shielding and use of a home-made Al-foil sample can.

A room temperature diffraction pattern was satisfactorily refined in the $I4_1/acd$ (#142) space-group proposed by Crawford *et al* [32]. Below the transition temperature ∼240 K, an extremely weak but statistically significant additional reflection was detected at the position consistent with the (1, 1, 1) propagation vector (figure 3 inset). Observation of this magnetic signal in combination with a quantitative Rietveld refinement (figure 3) allowed us to unambiguously confirm P_Icca ($I_pb'ca$) as the appropriate magnetic space-group, with an M_4 motif of magnetic dipoles depicted on the right in figure 2. The magnetic form-factor parameters for Ir^{4+} ions used in the refinement were taken from the recent pseudo-relativistic Hartree–Fock calculations made by Kobayashi *et al* [33], together with independent relativistic calculations by Desclaux [34].

As discussed in section 3.1, magnetic symmetry P_Icca ($I_pb'ca$) implies the presence of two orthogonal motifs, $+, -, +, -$ along the a-axis and $+, +, -, -$ along the b-axis. The refinement procedure on data collected with a sample temperature of 1.6 K yields the statistically significant value 0.24(4) μ_B only for the magnetic moment along the a-axis. The presence of a second mode, along the b-axis, does not directly follow from neutron diffraction data but an admixture of this component is expected based on magnetic symmetry, which allows a bilinear coupling between the associated order parameters via antisymmetric Dzyaloshinskii–Moriya exchange. Moreover, the experimental observation of the $(0, 0, 2n+1)$ reflections in resonant x-ray scattering, discussed in the previous section, testifies to the presence of a motif $+, +, -, -$. Our neutron diffraction data gives the upper limit for this component to be 0.17 μ_B, which means that the total ordered moment of the Ir^{4+} ions in Sr_2IrO_4 does not exceeds the value 0.29(4) μ_B.

4. Na_2IrO_3

Space-group $C2/m$ (#12, unique axis b), monoclinic and a centrosymmetric crystal-class C_{2h} $(2/m)$ with C-centring $(\frac{1}{2}, \frac{1}{2}, 0)$. Ir ions occupy sites 4(g) that possess a diad axis of rotation symmetry parallel to the b-axis, C_{2b}, and ions are at sites $0, y, 0; 0, -y, 0$. Choi *et al* [8] and Ye *et al* [10] agree that the general coordinate $y = 0.333$.

A point group C_{2b} confines dipoles to lay along the b-axis. However, Lovesey and Dobrynin [15] have demonstrated, beyond reasonable doubt, that magnetic dipoles are normal to the b-axis, and the appropriate point group is $C'_{2b} \equiv \theta C_{2b}$. In this case, all $\langle T^K_Q\rangle$ are purely real, with $\langle T^1_b\rangle = 0$. In addition, magnetic charge is forbidden while the anapole is normal to the b-axis.

4.1. Resonant x-ray Bragg diffraction

Resonant x-ray Bragg diffraction data for the honeycomb-lattice layered perovskite have been reported by Liu *et al* [6] and reflections indexed on the space-group $C2/c$. This space-group is revised to $C2/m$ by Choi *et al* [8], for which magnetic reflections (h, k, l) have Miller indices h, k integer and l half-integer. Reflections $h + k$ odd observed by Liu *et al* [6] are space-group forbidden.

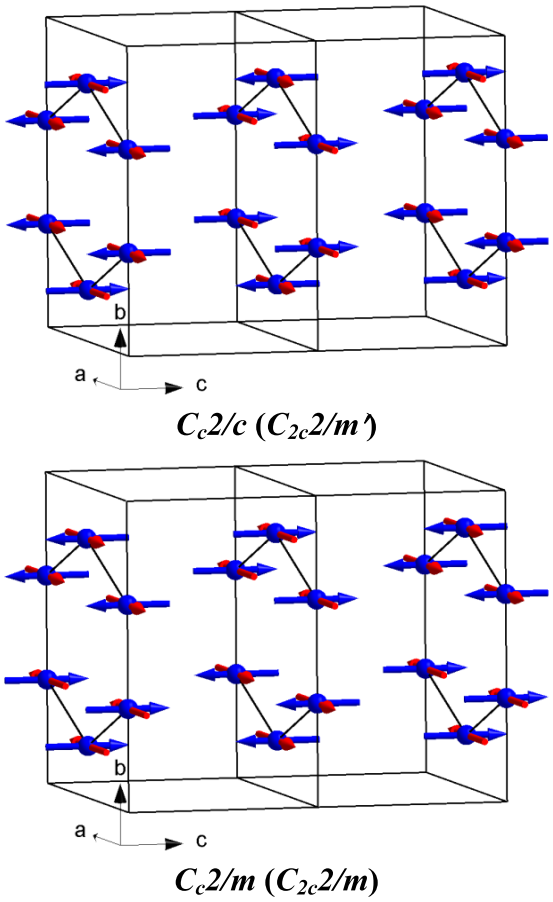

Figure 4. Na_2IrO_3; magnetic dipole components normal to the *b*-axis associated with M_2^+ (top) and M_2^- (bottom) irreps.

With space-group $C2/m$ and magnetic propagation vector $(0, 1, \frac{1}{2})$, there are two possible irreps M_2^+ and M_2^- transforming magnetic dipoles in the *a*–*c* plane with the corresponding magnetic space-groups C_c2/c ($C_{2c}2/m'$) and C_c2/m ($C_{2c}2/m$). Each irrep has two sets of basis functions (magnetic modes), meaning that the direction of magnetic dipoles within the *a*–*c* plane is not fixed by symmetry and can be arbitrary (figure 4). Since there are no symmetry reasons, the magnetic dipoles are very unlikely to be exactly along the *a*-axis. Lovesey and Dobrynin [15] point out that data reported by Liu *et al* [6] are unequivocal evidence for $\langle T_c^1 \rangle$ different from zero. The pattern of magnetic dipoles labelled zig-zag by Choi *et al* and Ye *et al* corresponds to M_2^-.

In M_2^+ environments at sites $0, y, 0$ and $0, -y, 0$ are related by inversion, I, and thus the motif of magnetic dipoles is $+, +$. The structure factor for electronic properties of iridium ions is readily found to be,

$$M_2^+; \Psi_Q^K = [1 + \sigma_\theta(-1)^{h+k}][\exp(\mathrm{i}\varphi) + \sigma_\pi \exp(-\mathrm{i}\varphi)]\langle O_Q^K \rangle, \quad (4.1)$$

where $\langle O_Q^K \rangle$ is the multipole for site $0, y, 0$, and $\varphi = 2\pi ky$. The signature σ_θ arises from an anti-translation element in the magnetic motif, and its presence in Ψ_Q^K is justified by the observation of diffraction at $(0, -1, \frac{11}{2})$, and related reflections, absent if $\sigma_\theta = +1$. The point group determines the relation between Ψ_{-Q}^K and Ψ_Q^K, and $\Psi_{-Q}^K = (-1)^Q \Psi_Q^K$ for all K and $\sigma_\pi = +1$, with Ψ_Q^K purely real. The identity $\Psi_{-Q}^K = (-1)^Q \Psi_Q^K$ holds for M_2^-, in which environments are related by a product of time reversal and inversion, θI, leading to a magnetic motif $+, -$, and a structure factor,

$$M_2^-; \Psi_Q^K = [1 + \sigma_\theta(-1)^{h+k}][\exp(\mathrm{i}\varphi) + \sigma_\theta\sigma_\pi \exp(-\mathrm{i}\varphi)]\langle O_Q^K \rangle. \quad (4.2)$$

Looking at the two structure factors (4.1) and (4.2), appropriate for M_2^+ and M_2^-, they differ only with respect to a dependence on Miller index k through the phase angle $\varphi = 2\pi ky$, which will either be $\cos(\varphi)$ or $[\mathrm{i}\sin(\varphi)]$ for magnetic diffraction ($\sigma_\theta = -1$) and an E1–E1 event ($\sigma_\pi = +1$).

Unit-cell structure factors for diffraction enhanced by an E1–E1 event are discussed by Lovesey and Dobrynin [15] in the context of diffraction data collected for a single value of $|k|$, namely $(0, \pm 1, l)$ with l half-integer, in which case it is not possible to distinguish between M_2^+ and M_2^- using resonant x-ray Bragg diffraction.

5. $Sr_3Ir_2O_7$

Space-group *Bbcb* (#68 origin choice 1), orthorhombic (alternative setting of *Ccca* derived using the transform $abc \to bca$), and centrosymmetric crystal-class D_{2h} (*mmm*) with *B*-centring $(\frac{1}{2}, 0, \frac{1}{2})$ [25]. Ir ions on sites 8(e) with point group C_{2c}, with four Ir ions at sites $0, 0, z$; $\frac{1}{2}, 0, \frac{1}{2} - z$; $\frac{1}{2}, \frac{1}{2}, -z$; $0, \frac{1}{2}, \frac{1}{2}+z$. The general coordinate $z = 0.097$ [26].

From $C_{2c}\langle O_Q^K \rangle = (-1)^Q \langle O_Q^K \rangle = \langle O_Q^K \rangle$ it follows that Q is even for both values of σ_π. Whence, dipoles $\langle O_a^1 \rangle = \langle O_b^1 \rangle = 0$, and magnetic charge is allowed in an E1–*M*1 event. Like $\langle \mathbf{T}^1 \rangle$, the anapole, $\langle \mathbf{G}^1 \rangle$, is parallel to the *c*-axis but it does not contribute to diffraction with $k + l$ even. $Sr_3Ir_2O_7$ is a bilayer variant of the single layer Sr_2IrO_4, which is the subject of section 3, and the two iridates support orthogonal alignments of Ir magnetic dipoles.

5.1. Resonant x-ray Bragg diffraction

Diffraction data enhanced at L_2 and L_3 absorption edges have been published by Kim *et al* [11] for reflections (h, k, l) with integer Miller indices, and conditions $h + k$ odd and $h + l$ odd ($k+l$ even) that are space-group forbidden. Our analysis shows that the magnetic propagation vector is (1, 0, 0), with two candidates for the magnetic space-group P_ccca ($C_pc'ca$) or P_Aban (C_pcca) associated with the one-dimensional irreps Y_3^+ and Y_1^-, respectively (figure 5). The latter is shown to be the correct choice by appealing to data for integrated intensities as a function of Miller index l that is displayed in figure 6.

For Y_3^+ environments relative to $0, 0, z$ are derived with C_{2b}, θI and θIC_{2b}, respectively, and the corresponding motif of dipole moments is $+, -, -, +$. Employing an

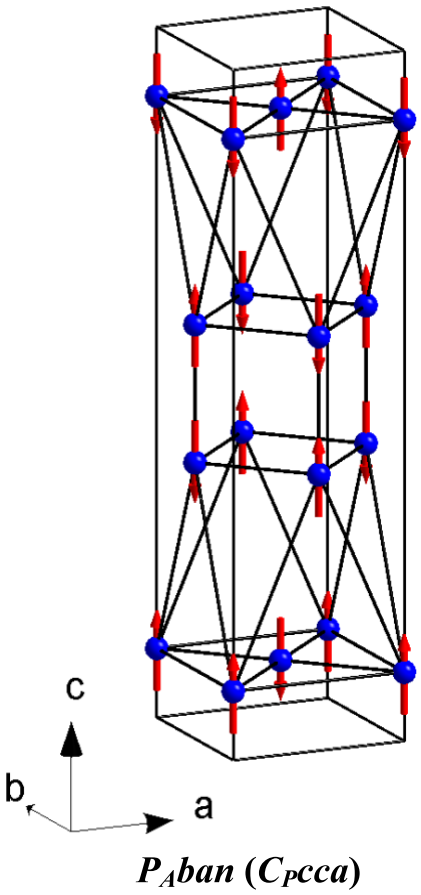

Figure 5. $Sr_3Ir_2O_7$; magnetic dipole configuration associated with Y_1^- irrep.

anti-translation and Q even, the electronic structure factor is,

$$Y_3^+;\ \Psi_Q^K = [1+\sigma_\theta(-1)^{h+l}][\exp(\mathrm{i}\varphi) + \sigma_\theta\sigma_\pi(-1)^{h+k}\exp(-\mathrm{i}\varphi)] \times [\langle O_Q^K\rangle + \sigma_\theta\sigma_\pi(-1)^{k+l+K}\langle O_{-Q}^K\rangle], \quad (5.1)$$

where the first factor expresses a restriction on Miller indices from an anti-translation element, and we find $\Psi_{-Q}^K = \sigma_\theta\sigma_\pi(-1)^{k+l+K}\Psi_Q^K$. The phase angle $\varphi = 2\pi lz$. Turning to the second candidate, Y_1^-, environments relative to $0, 0, z$ are derived with $\theta C_{2b}, I$ and θIC_{2b}, respectively, and the corresponding motif of dipole moments is $+, +, +, +$. The remaining four environments are generated by application of time reversal, θ, that creates a motif with opposite polarizations and $-$ replaces $+$. The electronic structure factor is,

$$Y_1^-;\ \Psi_Q^K = [1+\sigma_\theta(-1)^{h+l}] \times [\exp(\mathrm{i}\varphi) + \sigma_\pi(-1)^{h+k}\exp(-\mathrm{i}\varphi)] \times [\langle O_Q^K\rangle - \sigma_\pi(-1)^{k+l+K}\langle O_{-Q}^K\rangle]. \quad (5.2)$$

Time-even multipoles ($\sigma_\theta = +1$) do not contribute at reflections $h + l$ odd studied by Kim *et al* [11], and observed intensity will vanish with increasing temperature and loss of magnetic order.

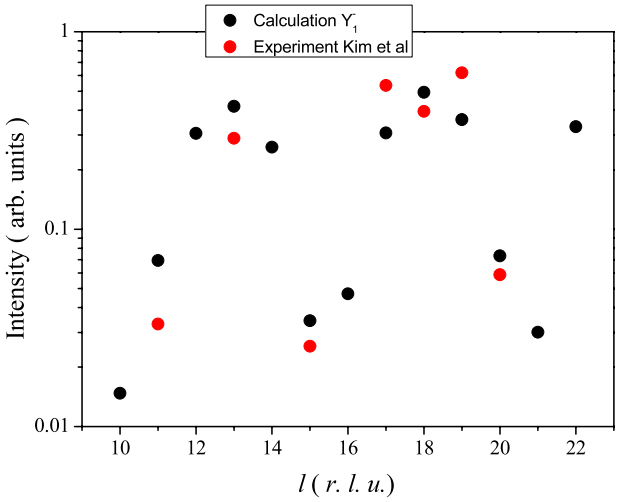

Figure 6. $Sr_3Ir_2O_7$; integrated intensity in the $\pi'\sigma$ channel of scattering as a function of Miller index l for reflections $(1, 0, l)$ with l even and $(0, 1, l)$ with l odd. Experimental data from Kim *et al* [11] are shown by red points. Black points are proportional to $[\sin\varphi\sin(\theta-\alpha)]^2$ which is the intensity variation predicted for irrep Y_1^-, P_Aban (C_Pcca) with an azimuthal angle $\psi = 180°$. An overall scale factor is the only fitting parameter between experimental data and the simulation.

We specialize to $\sigma_\pi = +1$, and construct corresponding unit-cell structure factors. With $h + l$ odd and $k + l$ even we satisfy conditions in the resonant x-ray Bragg diffraction experiment and find,

$$Y_3^+;\ \Psi_Q^K = 4\cos\varphi[\langle T_Q^K\rangle + \langle T_{-Q}^K\rangle], \quad (5.3)$$

and,

$$Y_1^-;\ \Psi_Q^K = 4\mathrm{i}\sin\varphi[\langle T_Q^K\rangle + \langle T_{-Q}^K\rangle], \quad (5.4)$$

where Q is even and K odd, i.e., non-magnetic scattering is forbidden and $F(\mathrm{E1–E1})_{\sigma'\sigma} = 0$.

Euler angles α, β, γ define the setting of the crystal at the origin of an azimuthal-angle scan, $\psi = 0$, defined in figure 1, where ψ is the angle of rotation of the crystal about the Bragg wavevector $(h, k, l) = h\mathbf{a}^* + k\mathbf{b}^* + l\mathbf{c}^*$. By definition [16, 17],

$$A_Q^K + B_Q^K = \exp(\mathrm{i}Q\alpha)\sum_q d_{Q,q}^K(\beta)\exp(\mathrm{i}q\gamma)\Psi_q^K, \quad (5.5)$$

with $q = 0, \pm1, \ldots, \pm K$ in the general case, and $d_{Q,q}^K(\beta)$ an element of the Wigner rotation matrix. For the case in hand K is odd and q even.

Let the unit vector $(t_1, t_2, t_3) = (h, k, l)/|(h, k, l)|$ For $(h, 0, l)$ with $\mathbf{a}^*$ in the plane of scattering, $\sin(\alpha) = t_1$, $\cos(\alpha) = -t_3$ and $\beta = \gamma = \pi/2$. One finds $A_0^1 = 0$, and A_1^1 and B_1^1 proportional to $\Psi_0^1 = 8\langle T_c^1\rangle$ and purely real. Whence,

$$Y_3^+;\ F(\mathrm{E1–E1})_{\pi'\sigma} = -\mathrm{i}4\sqrt{2}\langle T_c^1\rangle\cos\varphi[\sin\theta\cos\alpha + \cos\theta\sin\alpha\cos\psi], \quad (5.6)$$
$$F(\mathrm{E1–E1})_{\pi'\pi} = -\mathrm{i}4\sqrt{2}\langle T_c^1\rangle\cos\varphi\sin(2\theta)\sin\alpha\sin\psi,$$

and,

$$Y_1^-;\ F(\text{E1–E1})_{\pi'\sigma} = 4\sqrt{2}\langle T_c^1\rangle \sin\varphi[\sin\theta\cos\alpha + \cos\theta\sin\alpha\cos\psi],$$
$$F(\text{E1–E1})_{\pi'\pi} = 4\sqrt{2}\langle T_c^1\rangle \sin\varphi\sin(2\theta)\sin\alpha\sin\psi, \quad (5.7)$$

together with $F(\text{E1–E1})_{\sigma'\sigma} = 0$. Turning to reflections $(0, k, l)$ with $\mathbf{b}^*$ in the plane of scattering at $\psi = 0$, $\sin(\alpha) = t_2$, $\cos(\alpha) = -t_3$, $\beta = \pi/2$ and $\gamma = 0$. The foregoing unit-cell structure factors, calculated for $(h, 0, l)$, are the correct ones for $(0, k, l)$ upon using appropriate values of θ and α. For both types of reflection there is no diffraction at the origin of the azimuthal-angle scan, $\psi = 0$, in the unrotated channel of scattering, $\pi'\pi$. In this polarization channel, diffraction by magneto-electric multipoles is also proportional to $\sin(\psi)$ and, consequently, it is not the origin of the small intensity reported by Kim *et al* [11].

Integrated intensity in the $\pi'\sigma$ channel of scattering as a function of Miller index l is proportional to $[\cos\varphi\sin(\theta\pm\alpha)]^2$ for Y_3^+ and $[\sin\varphi\sin(\theta\pm\alpha)]^2$ for Y_1^-, where the two signs are for $\psi = 180°$ $(-)$ and $\psi = 0°$ $(+)$. All three angles, φ, θ and α, are functions of Miller index l. Data reported by Kim *et al* [11], reproduced in figure 6, are seen to be well represented by $[\sin\varphi\sin(\theta-\alpha)]^2$. We conclude for the iridate $Sr_3Ir_2O_7$ that the magnetic motif is Y_1^-, P_Aban (C_pcca) with propagation vector (1, 0, 0). The configuration of dipole moments is the same as that depicted by Kim *et al* [11], although the propagation vector is not (0, 0, 0) quoted by the authors. It is notable that our simulation of intensity of Y_1^-, namely $[\sin\varphi\sin(\theta\pm\alpha)]^2$, shows remarkable differences for $\psi = 180°$ $(-)$ and $0°$ $(+)$, with $[\sin(\theta-\alpha)]^2/[\sin(\theta+\alpha)]^2 = 55.0$ at $l = 13$. Using figure 1, a setting $\psi = 180°$ places the a-axis mostly along $\mathbf{q} + \mathbf{q}'$ for reflections $(1, 0, l)$ and l large and even, and the b-axis mostly along $\mathbf{q} + \mathbf{q}'$ for $(0, 1, l)$ and l large and odd.

Finally, we point out that the magnetic symmetry P_Aban (C_pcca) deduced with the foregoing arguments does not allow a weak ferromagnetic component. Observation of the latter is reported; see, for instance, [28, 29]. This inconsistency most probably relates to the crystal structure symmetry which must be different from *Bbcb*. This space-group was deduced as a possible distorted variant of the parent $I4/mmm$ symmetry with the $(\frac{1}{2}, \frac{1}{2}, 0)$ propagation vector (X-point of symmetry). Considering others isotropy subgroups of $I4/mmm$ with this propagation vector, we found that the magnetic motif shown in figure 5 in combination with either *Cmcm* or *Cmma* crystal structure symmetry will result in the $Cm'cm'$ or $Cm'm'a$, magnetic space-groups, respectively, which allow in-plane weak ferromagnetic component. Thus, more experimental efforts are necessary to reinvestigate the crystal structure of $Sr_3Ir_2O_7$ and make it consistent with the observed physical properties.

5.2. Iridium ground-state wavefunction

Much is written about the role of a $J_{\text{eff}} = \frac{1}{2}$ state in explaining novel features of iridates [1–15]. It is composed entirely of 5d electron states with total angular momentum $j = \frac{5}{2}$, states that do not contribute to diffraction enhanced by the L_2 absorption edge, because they violate selection rules for an E1–E1 event. Hence, experimental observation of next to no intensity at the L_2 absorption edge might be viewed as evidence of an electron state dominated by $J_{\text{eff}} = \frac{1}{2}$. It has been shown in the case of Sr_2IrO_4 that zero intensity at the L_2 absorption edge can be achieved with an iridium state that contains $j = \frac{3}{2}$, meaning that said state is assuredly not $J_{\text{eff}} = \frac{1}{2}$ [14]. Magnetic dipole moments in Sr_2IrO_4 are normal to the c-axis. Here we re-visit the argument for zero intensity at the L_2 absorption edge using $j = \frac{3}{2}$ for dipoles parallel to the c-axis, which is appropriate for $Sr_3Ir_2O_7$. We conclude that $\langle T_c^1\rangle_{L2} = 0$ is possible with an iridium ground-state that includes states $j = \frac{3}{2}$ and, consequently, the state is not $J_{\text{eff}} = \frac{1}{2}$.

Let one component of a Kramers doublet be,

$$|u\rangle = \sum_{j,m} \Gamma(j, m)|j, m\rangle, \qquad \text{with}$$
$$\sum_{j,m} |\Gamma(j, m)|^2 = 1, \quad (5.8)$$

where $j = \frac{3}{2}$ and $\frac{5}{2}$ for a d-state, and $\Gamma(j, m)$ are coefficients with properties to be determined. The second component of the doublet $|v\rangle = \theta|u\rangle$ is constructed from $|u\rangle$ with a standard convention $\theta(\Gamma(j, m)|j, m\rangle) = (-1)^{j-m}\Gamma(j, m)^*|j, -m\rangle$. A trial ground-state $[f|v\rangle + |u\rangle]/\sqrt{(1 + |f|^2)}$, with a complex mixing parameter f, gives for the expectation value $\langle T_c^K\rangle = \langle T_0^K\rangle$ of interest,

$$\langle T_0^K\rangle = (1 + |f|^2)^{-1} \sum_{j,j',m} \langle j, m|T_0^K|j', m\rangle \times [\Gamma(j, m)^*\Gamma(j', m) - |f|^2\Gamma(j, m)\Gamma(j', m)^* + (-1)^{j'+m}\{f\Gamma(j, m)^*\Gamma(j', -m)^* + f^*\Gamma(j, m)\Gamma(j', -m)\}], \quad (5.9)$$

with K odd, and the matrix element $\langle j, m|T_0^K|j', m\rangle$ purely real. Coefficients $\Gamma(j, m)$ and f are chosen to meet the requirement that $\langle T_0^K\rangle$ is purely real. Contributions proportional to f are purely real for arbitrary $\Gamma(j, m)$ and f. Remaining contributions to $\langle T_0^K\rangle$ must obey $\text{Im}[\Gamma(j, m)^*\Gamma(j', m)] = 0$. We satisfy this condition in the simplest manner and choose all $\Gamma(j, m)$ purely real and go on to find,

$$\langle T_0^K\rangle = (1 + |f|^2)^{-1} \sum_{j,j',m} \langle j, m|T_0^K|j', m\rangle \times [(1 - |f|^2)\Gamma(j, m)\Gamma(j', m) + 2f'(-1)^{j'+m}\Gamma(j, m)\Gamma(j', -m)], \quad (5.10)$$

where $f' = \text{Real}\, f$.

Next, we specialize to the L_2 absorption edge, for which the matrix element $\langle j, m|T_0^K|j', m\rangle = 0$ unless $j = j' = \frac{3}{2}$, and a magnetic dipole ($K = 1$),

$$\langle T_0^1\rangle_{L2} = [18\sqrt{2}(1 + |f|^2)]^{-1} \times [(|f|^2 - 1)\{3\Gamma(j, \tfrac{3}{2})^2 - 3\Gamma(j, -\tfrac{3}{2})^2 + \Gamma(j, \tfrac{1}{2})^2 - \Gamma(j, -\tfrac{1}{2})^2\} + 4f'\{3\Gamma(j, \tfrac{3}{2})\Gamma(j, -\tfrac{3}{2}) - \Gamma(j, \tfrac{1}{2})\Gamma(j, -\tfrac{1}{2})\}], \quad (5.11)$$

with $j = \frac{3}{2}$. Our expression for $\langle T^1_0\rangle_{L2}$ is quite general apart from selecting purely real coefficients rather than some other, more complicated, choice of coefficients that satisfy $\mathrm{Im}[\Gamma(j,m)^*\Gamma(j,m)] = 0$. A similar calculation reveals that the requirement $\langle T^1_{\pm1}\rangle_{L2} = 0$ is met for $f = 1$ and coefficients that obey the identity,

$$\langle T^1_{\pm1}\rangle_{L2} \propto \Gamma(j,-\tfrac{1}{2})[\sqrt{3}\Gamma(j,\tfrac{3}{2}) + \Gamma(j,-\tfrac{1}{2})] - \Gamma(j,\tfrac{1}{2})[\sqrt{3}\Gamma(j,-\tfrac{3}{2}) + \Gamma(j,\tfrac{1}{2})] = 0. \quad (5.12)$$

If $\sqrt{3}\Gamma(j,\frac{3}{2}) + \Gamma(j,-\frac{1}{2}) = 0$ and $\sqrt{3}\Gamma(j,-\frac{3}{2}) + \Gamma(j,\frac{1}{2}) = 0$ we see that $\langle T^1_0\rangle_{L2}$ and $\langle T^1_{\pm1}\rangle_{L2}$ are both zero, using $f = 1$. Another example is one coefficient with $m = \pm\frac{3}{2}$ different from zero, akin to the case encountered for Sr_2IrO_4 [14]. At the L_3 absorption edge, $\langle T^1_0\rangle_{L3}$ need not be zero because it depends on products $\Gamma(\frac{3}{2},m)\Gamma(\frac{5}{2},m')$ and $\Gamma(\frac{5}{2},m)\Gamma(\frac{5}{2},m')$ while conditions apply to $\Gamma(\frac{3}{2},m)$ in order that contributions $\Gamma(\frac{3}{2},m)\Gamma(\frac{3}{2},m')$ lead to $\langle \mathbf{T}^1\rangle_{L2} = 0$.

6. $CaIrO_3$

Space-group *Cmcm* (#63), orthorhombic, centrosymmetric crystal-class D_{2h} (*mmm*) with *C*-centring $(\frac{1}{2},\frac{1}{2},0)$. Crystal physics of the layered post-perovskite $CaIrO_3$ is thoroughly reviewed by Cheng *et al* [12]. In the chemical structure Ir ions use sites 4(a) that are centres of inversion symmetry with a diad axis of rotation symmetry parallel to the *a*-axis, C_{2a}. Ions occupy sites 0, 0, 0; 0, 0, $\frac{1}{2}$ that are centres of inversion symmetry.

To match observations made with resonant x-ray Bragg diffraction [13], we find it is necessary to invoke the symmetry of an odd diad $C'_{2a} \equiv \theta C_{2a}$ that confines magnetic dipoles to the *b*–*c* plane, while sites used by Ir ions remain centres of inversion symmetry. In addition, environments at positions 0, 0, 0 and 0, 0, $\frac{1}{2}$ differ by a two-fold rotation about the *b*-axis, C_{2b}, creating a motif +, − for magnetic dipoles aligned along the *c*-axis. In the chemical structure and a point group $2/m$, C_{2b} is equivalent to $C_{2c} = C_{2b}C_{2a}$ but this is no longer the case with magnetic order. Because a centre of inversion symmetry exists, we need consider only parity-even multipoles, with $\sigma_\theta = (-1)^K$, that satisfy $\langle T^K_Q\rangle = \theta C_{2a}\langle T^K_Q\rangle = \langle T^K_{-Q}\rangle$ resulting in the identity $\langle T^K_Q\rangle = (-1)^Q\langle T^K_Q\rangle^*$.

6.1. Resonant x-ray Bragg diffraction

Resonant x-ray diffraction has been reported by Ohgushi *et al* [13]. Intensity is observed at space-group forbidden reflections $(0,0,l)$ with l an odd integer. Templeton and Templeton scattering by electric quadrupoles ($K = 2$) with angular anisotropy is allowed [27], as we shall see.

A short calculation leads to an electronic structure factor,

$$\Psi^K_Q = [1 + (-1)^{h+k}][1 + (-1)^l C_{2b}]\langle T^K_Q\rangle = [1 + (-1)^{h+k}][\langle T^K_Q\rangle + (-1)^l(-1)^{K+Q}\langle T^K_{-Q}\rangle], \quad (6.1)$$

and it can be different from zero for $h+k$ even. Bulk electronic properties are described by Ψ^K_Q with $h = k = l = 0$. One finds

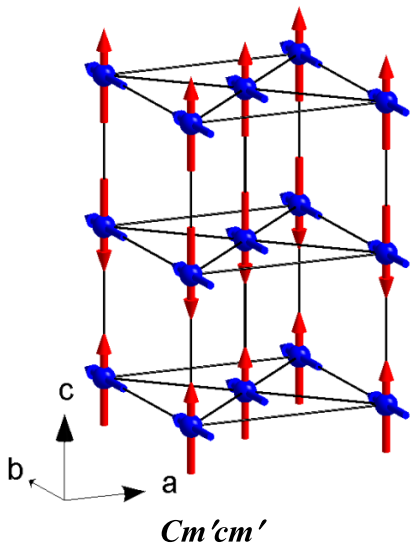

Figure 7. $CaIrO_3$; magnetic dipole components transforming according to the Γ^+_4 irrep.

$\Psi^1{}_0 = 0$, and $\Psi^1{}_{+1}$ proportional to $\langle T^1_b\rangle$ showing that there is a ferromagnetic component to the magnetization parallel to the *b*-axis. Again using $h+k$ even but with l odd, for magnetic Bragg diffraction, the result $\Psi^K_Q = 2[1 - (-1)^{K+Q}]\langle T^K_Q\rangle = \Psi^K_{-Q}$ gives the condition $K + Q$ odd.

$CaIrO_3$ is a simple case of a weak ferromagnet, when both antiferromagnetic and ferromagnetic patterns of magnetic dipoles have identical symmetry and therefore must be coupled together. With magnetic dipoles normal to the *a*-axis there are two candidate magnetic groups, with magnetic propagation vector 0 at the Γ-point of symmetry. These are, $Cm'c'm$ associated with Γ^+_2 irrep and $Cm'cm'$ associated with Γ^+_4 irrep that are distinguished by ferromagnetic components parallel to the *c*-axis and *b*-axis, respectively. The latter, depicted in figure 7, is a property of the iridate under consideration, and thus we have an unambiguous assignment $Cm'cm'$ for $CaIrO_3$.

For reflections $(0,0,l)$ Euler angles in (5.5) are $\alpha = \pi$, $\beta = \pi/2$ and $\gamma = 0$. With l odd all A^K_Q are zero, leading to $F(\mathrm{E1–E1})_{\sigma'\sigma} = F(\mathrm{E1–E1})_{\pi'\pi} = 0$. Contributions B^K_Q to $F(\mathrm{E1–E1})_{\pi'\sigma}$ are B^1_1 and B^2_2 which yield,

$$F(\mathrm{E1–E1})_{\pi'\sigma} = 2[\mathrm{i}\sqrt{2}\sin\theta\langle T^1_c\rangle + 2\cos\theta\sin\psi\langle T^2_{+1}\rangle'']. \quad (6.2)$$

We conclude that, contributions to diffraction by the magnetic dipole, $\langle T^1_c\rangle$, and non-magnetic quadrupole are 90° out of phase, whence intensity $|F(\mathrm{E1–E1})_{\pi'\sigma}|^2$ as a function of azimuthal angle is $\cos(2\psi)$ plus a constant. It is notable that, the dipole parallel to the *b*-axis, $\langle T^1_b\rangle$, which creates a ferromagnetic motif, does not contribute to $F(\mathrm{E1–E1})_{\pi'\sigma}$ evaluated for reflections $(0,0,l)$ with Miller index l an odd integer. The quadrupole with angular anisotropy that generates Templeton and Templeton scattering $\langle T^2_{+1}\rangle'' = -\sqrt{(\frac{2}{3})}\langle T^2_{bc}\rangle$ in terms of Cartesian components. When $\psi = 0$ the crystal *b*-axis is in the plane of scattering and in the opposite direction to $\mathbf{q} + \mathbf{q}'$ (figure 1).

Dependence of $F(\text{E1–E1})_{\pi'\sigma}$ in result (6.2) on θ and ψ agrees with a result quoted by Ohgushi *et al* [13]. However, the authors do not specify any properties of the magnetic and non-magnetic contributions to scattering, shown here to be a dipole $\langle T^1_c \rangle$ and a quadrupole $\langle T^2_{bc} \rangle$, respectively.

Energy profiles observed at the L_3 absorption edge, where most data were collected [13], show several distinct, closely spaced contributions, which is not so for the other three iridates [4, 6, 7, 11]. This added complexity gives more weight to the value of results derived from crystal symmetry, since they surmount such complexity. Ohgushi *et al* [13] report very weak intensities at the L_2 absorption edge. This finding, of next to no intensity at L_2, and our result for the magnetic point group, C'_{2a}, imposes restrictions on the iridium wavefunction. The necessary steps are akin to exercises reported for $Sr_3Ir_2O_7$, section 5.2, and Sr_2IrO_4 [14].

7. Discussion

Magnetic properties of the iridates Sr_2IrO_4, Na_2IrO_3, $Sr_3Ir_2O_7$ and $CaIrO_3$ are discussed taking account of recently published data for Bragg intensities observed in resonant x-ray diffraction. The experimentalists chose iridium atomic resonances, L_2 and L_3, in order that intensities relate directly to 5d valence states, and charge, spin and orbital electronic degrees of freedom therein may be observed.

Bragg intensities are here simulated with an atomic model—using multipoles constructed from the electronic ground-state of an iridium ion—that is well-suited to make best use of symmetry. Our electronic structure factors serve the immediate purpose, of interpreting x-ray Bragg intensities, but are also a platform on which to interpret future investigations using, say, dichroic signals, resonant x-ray diffraction or neutron diffraction [16]. Multipoles we identify as giving rise to diffracted intensity can be estimated with *ab initio* methods of calculating electronic structure.

Magnetic space-groups are considered for each compound. For two compounds, $Sr_3Ir_2O_7$ and $CaIrO_3$, published x-ray data permit us to assign a magnetic space-group, while for Na_2IrO_3 there are simple reasons for indecision that we delineate. A complete description of Sr_2IrO_4 with magnetic propagation vector (1, 1, 1) is accomplished using published x-ray diffraction data in conjunction with our own high-resolution data gathered on a powder sample by neutron diffraction. In all cases, configurations of magnetic dipoles are depicted in cartoons.

Some aspects of the magnetic properties of Sr_2IrO_4 and Na_2IrO_3 are covered in previous publications, [14] and [15], respectively. In the case of Sr_2IrO_4 we here conclude that, the magnetic space-group P_Icca ($I_pb'ca$) is consistent with reflection conditions present in resonant x-ray and neutron diffraction data (magnetic space-groups are given in the Belov–Neronova–Smirnova and Opechowski–Guccione (in brackets) notations). Magnetic space-groups C_c2/c ($C_{2c}2/m'$) and C_c2/m ($C_{2c}2/m$) are shown to be consistent with currently available resonant x-ray diffraction data for Na_2IrO_3.

$Sr_3Ir_2O_7$ is discussed using space-group *Bbcb* for the crystal structure. Our study of resonant diffraction data leads to the assignment P_Aban (C_pcca) with propagation vector (1, 0, 0). To this end, we must confront data for the integrated intensity in a channel with rotated polarization ($\pi'\sigma$) as a function of Miller index l with a simulation. In this exercise, we achieve a quality of fit superior to that already published and, in addition, our propagation vector is not the (0, 0, 0) quoted by the same authors [14]. It is noteworthy that, a magnetic symmetry P_Aban (C_pcca) does not allow a weak ferromagnetic component that has been reported [28, 29]. This apparent inconsistency most probably relates to the crystal structure symmetry which must be different from *Bbcb*, and there is a case for refinement to our knowledge of the crystal structure.

Additional work on $Sr_3Ir_2O_7$ is directed at an improved knowledge of the Ir wavefunction. This entails imposing constraints on the wavefunction to comply with point-group symmetry and a calculation of Ir dipoles observed at L_2 and L_3 absorption edges. It is shown that a much-discussed candidate for the Ir wavefunction, labelled $J_{\text{eff}} = \frac{1}{2}$ [1, 4, 11], is not a certain favourite.

Bulk magnetization and resonant x-ray Bragg diffraction data [13] lead us to assign $Cm'cm'$ for the magnetic space-group of $CaIrO_3$, a simple case of a weak ferromagnet. Moreover, we are able to specify the exact nature of the magnetic (time-odd) dipole and electric (Templeton and Templeton scattering and time-even) quadrupole engaged in diffraction.

Acknowledgments

One of us (SWL) continues to be grateful to Dr K S Knight for insights to the physical properties of crystals. Dr J-P Desclaux provided atomic form factors for Ir^{4+} used in our analysis of neutron diffraction data. Professor E Balcar prepared figure 1. We thank Professor K Ohgushi for correspondence on his studies of $CaIrO_3$ [13]. The work at the University of Kentucky was supported by NSF through grants DMR-0856235 and EPS-0814194.

References

[1] Kim B J *et al* 2008 *Phys. Rev. Lett.* **101** 076402
[2] Jackeli G and Khaliullin G 2009 *Phys. Rev. Lett.* **102** 017205
[3] Shitade A *et al* 2009 *Phys. Rev. Lett.* **102** 256403
[4] Kim B J *et al* 2009 *Science* **323** 1329
[5] Singh Y and Gegenwart P 2010 *Phys. Rev.* B **82** 064412
[6] Liu X *et al* 2011 *Phys. Rev.* B **83** 220403
[7] Boseggia S *et al* 2012 *Phys. Rev.* B **85** 184432
[8] Choi S K *et al* 2012 *Phys. Rev. Lett.* **108** 127204
[9] Singh Y *et al* 2012 *Phys. Rev. Lett.* **108** 127203
[10] Ye F *et al* 2012 *Phys. Rev.* B **85** 180403
[11] Kim J W *et al* 2012 *Phys. Rev. Lett.* **109** 037204
[12] Cheng J-G *et al* 2011 *Phys. Rev.* B **83** 064401
[13] Ohgushi K *et al* 2012 arXiv:1108.4523
[14] Chapon L C and Lovesey S W 2011 *J. Phys.: Condens. Matter* **23** 252201
[15] Lovesey S W and Dobrynin A N 2012 *J. Phys.: Condens. Matter* **24** 382201
[16] Lovesey S W *et al* 2005 *Phys. Rep.* **411** 233

[17] Scagnoli V and Lovesey S W 2009 *Phys. Rev.* B **79** 035111
[18] Lovesey S W and Scagnoli V 2009 *J. Phys.: Condens. Matter* **21** 474214
[19] Lovesey S W and Balcar E 2013 *J. Phys. Soc. Japan* at press
[20] Carra P *et al* 1993 *Physica* B **192** 182
[21] Lovesey S W and Balcar E 1997 *J. Phys.: Condens. Matter* **9** 8679
[22] Ishii K *et al* 2011 *Phys. Rev.* B **83** 115121
[23] Ament L J P *et al* 2011 *Phys. Rev.* B **84** 020403
[24] Lovesey S W and Balcar E 2010 *J. Phys. Soc. Japan* **79** 104702
[25] Shaked H *et al* 2000 *J. Solid State Chem.* **154** 361
[26] Subramanian M A, Crawford M K and Harlow R L 1994 *Mater. Res. Bull.* **29** 645
[27] Dmitrienko V E *et al* 2005 *Acta Crystallogr.* A **61** 481
[28] Cao G *et al* 2011 *Phys. Rev.* B **66** 214412
[29] Nagai I *et al* 2007 *J. Phys.: Condens. Matter* **19** 136214
[30] Stokes H T, Hatch D M and Campbell B J 2007 *ISOTROPY* [stokes.byu.edu/isotropy.html]
[31] Campbell B J, Stokes H T, Tanner D E and Hatch D M 2006 *J. Appl. Crystallogr.* **39** 607
[32] Crawford M K *et al* 1994 *Phys. Rev.* B **49** 9198
[33] Kobayashi K *et al* 2011 *Acta Crystallogr.* A **67** 473
[34] Desclaux J-P 2011 private communication